Syntheses and structure of the La_5Ge_3Z phases ($Z =$ Si, Sn, Pb, Ga, In): Structural relationships among the M_5X_4-type structures

Arnold Guloy[1], John D. Corbett[*]

Department of Chemistry and Ames Laboratory,[2] Iowa State University, Ames, Iowa 50011, USA

Abstract

The indicated reactions under arc-melting or high-temperature sintering conditions in Ta containers lead to (1) the apparent Zintl phase $La_5Ge_3Si_{0.75}$, stuffed Mn_5Si_3-type, $P6_3/mcm$ from quenching; (2) α-La_5Ge_3Si (Sm_5Ge_4-type, $Pnma$); (3) β-La_5Ge_3Si (Zr_5Si_4-type, $P4_12_12$) at high temperatures; (4) La_5Ge_3Tt, $Tt =$ Sn, Pb, phases isotypic with 2); and (5) the isotypic La_5Ge_3Tr, $Tr =$ Ga, In, (Gd_5Si_4-type, $Pnma$). The structures of compounds 3 and 5 (for $Tr =$ Ga) have been refined from single crystal X-ray diffraction data. A general description of the three electron-poorer M_5X_4 structure types 2,3,4 (and of Eu_5As_4-type ($Cmca$)) is given in terms of their common building block, an La_9Tt_6 cubeoctahedra centered about the tightest bound La. Some electronic bonding effects are also generalized with regard to the dominance of extra free electrons beyond simple Zintl expectations.
© 2005 Published by Elsevier Inc.

Keywords: Crystal structures; La_5Ge_4 derivatives; Synthesis—La_5Ge_4 and derivatives; Comparison of M_5X_4 structure types; La_5Ge_3Si—synthesis and structures; La_5Ge_3Sn—synthesis and structure; La_5Ge_3Pb—synthesis and structure; $La_5Ge_3Si_{0.75}$—synthesis and structure; La_5Ge_3Ga—synthesis and structure

1. Introduction

Our earlier investigations of the "stuffed" Mn_5Si_3-type phases of La_5Ge_3 [1] demonstrated an apparent success of the Zintl–Klemm concept [2] in explaining structure–bonding property relationships. For example, in spite of the successful incorporation of fractional amounts of boron and carbon into La_5Ge_3, attempts to synthesize the fully stuffed Mn_5Si_3Z-type analogues with heavier group 14 and 13 interstitials elements were unsuccessful, rather other unrelated products were obtained instead. This is in fact reasonable inasmuch as our simple electron counting scheme indicates, and measurements prove, that the pnictide-stuffed derivatives such as La_5Ge_3As are closed shell semiconductors ($5 \times 3 - 3 \times 4 - 3 = 0$). The host La_5Ge_3 with isolated anions has only $15 - 12 = 3$ electrons available, and these are insufficient to completely fill the low-lying valence states of the electron-poorer interstitials of group 13 and 14 elements. Instead, these form products with closely related M_5X_4 phases that have the Zr_5Si_4 [3], Gd_5Si_4 [4], Sm_5Ge_4 [5] or perhaps Eu_5As_4 structure types [6]. These related structures all contain a common structural feature—X_2 dimers—as evident means to avoid an unfilled valence band of an Mn_5Si_3-type (or other) derivative. Individually, the 5–4 structures differ largely in the number of dimers per formula unit and how these dimers are arranged, and none appears electron precise. The Zr_5Si_4 and Gd_5Si_4 structures each

have two dimers per formula unit, whereas Sm_5Ge_4 and Eu_5As_4 each have one, with the other two main group members as monoanions. Recently, interest in 5–4 rare-earth-metal tetrelides (Tt = Si, Ge and Sn) has increased significantly owing to their unique magnetocaloric properties [7–9] and novel potential magnetic refrigeration applications [10–12].

This article reports on the syntheses, phase and structural relationships among different $La_5Ge_3Z_x$ phases in which Z is a group 13 or 14 element and which have either a stuffed-Mn_5Si_3 or one of the M_5X_4-type structures. The studies include the syntheses and structural data on three new phases: the substoichiometric phase $La_5Ge_3Si_{0.75}$ with the filled Mn_5Si_3 structure, a Zr_5Si_4-type structure for the fully stoichiometric La_5Ge_3 Si, and a Gd_5Si_4-type phase La_5Ge_3Ga in which further dimerization has evidently been forced by the reduced number of electrons introduced by gallium. Interrelationships among the four 5–4 structure types are also given consideration in terms of a general La_9Tt_6 model.

2. Experiment section

The general procedures have been previously described: high-temperature syntheses from high purity elements in welded Ta tubing, Guinier X-ray powder diffraction for both the identification of product phases and the determination of accurate lattice dimensions from indexed patterns, and general glovebox manipulations [1,13–14]. Structure types and cell dimensions for the phases studied are given in Table 1.

Syntheses of La_5Ge_3Z. Z = Silicon: Initial attempts to synthesize the presumed Zintl phase $La_5Ge_3Si_{0.75}$ from reactions of the elements at 1200 °C resulted in multi-

phase products that included Mn_5Si_3- and Sm_5Ge_4-type phases. However, a different approach, arc melting of the elements according to the stoichiometry

$$4La_5Ge_3 + 3Si \rightarrow 4La_5Ge_3Si_{0.75}$$
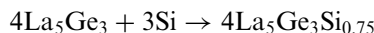
yielded a single-phase Mn_5Si_3-type product that represents the nominal limiting Zintl (valence) composition in the system La_5Ge_3Si ($5 \times 3 - 3 \times 4 - 0.75 \times 4 = 0$). However, annealing this as-cast button at 1100 °C resulted in disproportionation into $La_5(Ge,Si)_3$ and $La_5(Ge,Si)_4$-type phases according to powder diffraction patterns. The ternary 5–4 compound could be readily assigned to the Sm_5Ge_4 structure type but with understandably smaller unit cell parameters than those of La_5Ge_4 [15,16]. Indexing and refinement of lattice parameters from diffraction line positions for the Mn_5Si_3-type product yielded values close to those of binary La_5Ge_3 [1]. Although the standard deviations were not small enough to allow us to ascertain that the Mn_5Si_3-type product was indeed La_5Ge_3 and not $La_5Ge_{3-x}Si_x$ with small x, we concluded that the disproportionation reaction could be represented by something close to the reaction

$$La_5Ge_3Si_{0.75} \rightarrow 1/4\ La_5Ge_3 + 3/4\ La_5Ge_3Si.$$
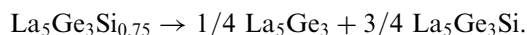
Equilibration of arc melted samples with nominal stoichiometries of $La_5Ge_3Si_x$, $0.2 < x \leqslant 0.75$, at 1100 °C resulted in the same behavior as that observed for $La_5Ge_3Si_{0.75}$, i.e., disproportionation of arc melted samples into mixtures of Mn_5Si_3- and Sm_5Ge_4-type phases. The relative amounts of the 5–3 phase decreased with an increase in silicon content as also observed directly following reactive sintering reactions. The annealing reaction for $x = 1.0$ resulted in a single phase sample (95% conservatively) of $(\alpha)La_5Ge_3Si$ with the Sm_5Ge_4 structure; see Table 1.

Table 1
Summary of structural data for La_5Ge_3Tt (Tt = Ge, Si, Sn, Pb) and La_5Ge_3Tr (Tr = Ga, In) phases

Composition	Synthesis conditions[a]	Lattice parameters[b]				Structure type[c]
		a	b	c	V	
La_5Ge_4	S	8.065(1)	15.474(2)	8.172(2)	1019.8(4)	Sm_5Ge_4
$La_5Ge_3Si_{0.75}$	A	8.937(1)		6.944(2)	480.2(2)	Mn_5Si_3[d]
α-La_5Ge_3Si	S	8.059(1)	15.454(1)	8.165(1)	1016.9(4)	Sm_5Ge_4
β-La_5Ge_3Si	A	8.148(1)		15.294(2)	1015.4(4)	Zr_5Si_4[d]
La_5Si_4	S	8.046(1)		15.432(1)	999.0(4)	Zr_5Si_4
La_5Ge_3Sn	S	8.156(1)	15.630(2)	8.292(1)	1057.0(4)	Sm_5Ge_4
La_5Ge_3Pb	S	8.176(1)	L5.625(2)	8.288(1)	1058.8(4)	Sm_5Ge_4
La_5Sn_4	S	8.435(1)	16.194(2)	8.630(1)	1178.7(5)	Sm_5Ge_4
La_5Pb_4	S	8.536(1)	16.314(2)	8.675(1)	1208.1(4)	Sm_5Ge_4
La_5Ge_3Ga	S	7.910(1)	15.294(2)	8.252(1)	998.3(4)	Gd_5Si_4
La_5Ge_3In	S	7.9099(8)	15.656(3)	8.2523(8)	1021.9(4)	Gd_5Si_4

[a]S: Sintering reactions of binaries and elements at 1100–1300 °C for 10–15 days; A: Arc melting of binaries and/or the elements.
[b]Å, Å^3.
[c]Sm_5Ge_4, *Pnma*; Mn_5Si_3, $P6_3/mcm$; Zr_5Si_4, $P4_12_12$; Gd_5Si_4, *Pnma*.
[d]Quenched high-temperature structures. The remainder all pertain to room temperature.

Arc-melting reactions of compositions $La_5Ge_3Si_x$, $0.75 < x < 1.0$, resulted in different and more complicated powder diffraction patterns in which some lines could be assigned to a Mn_5Si_3-type phase, whereas many others could not be completely indexed with a Sm_5Ge_4-type structure. These extra lines were also present in the powder pattern of as-cast La_5Ge_3Si in which no Mn_5Si_3-type phase was observed. However, upon annealing at 1100 °C, the samples $0.75 < x < 1.0$ transformed to what resembled an Sm_5Ge_4-type phase, as before, plus many of the lines corresponding to an Mn_5Si_3-type product. Rod-like crystals were observed growing out from the surface of the as-cast arc melted buttons with nominal compositions of La_5Ge_3Si, and these provided the opportunity to investigate the crystal structure of the new high temperature phase (β).

Tin and lead: The La_5Ge_3Si results led us to investigate the Sn and Pb analogues. The compounds La_5Ge_3Sn and La_5GePb, isostructural with α-La_5Ge_3Si (Sm_5Ge_4-type), were first obtained from mixtures heated in a high-temperature vacuum furnace. Since this furnace did not provide an adequate means to quench prospective high-temperature phases, and arc-melting routes did not give clean reactions with the more volatile Sn and Pb, quenching reactions were performed on samples sealed in tantalum containers and suspended within evacuated silica jackets. These were heated in tubular resistance furnaces to 1050 °C for 2 weeks and then quenched by dropping the jacketed containers into cold water. However, their powder diffraction patterns did not indicate any β-La_5Ge_3Si-like products, rather the patterns of all of the products, slow cooled or quenched, were those of the Sm_5Ge_4-type. Quenching the reactions from still higher temperatures were attempted within an induction furnace, the sealed tantalum containers at 1500 °C being quenched by the off-gas from liquid N_2 that was sucked into the evacuated reaction chamber. The results were unchanged; no β-La_5Ge_3Si-like phases was observed. As a final attempt to synthesize a high-temperature phase for Sn and Pb, prereacted La_5Ge_3Z compositions were arc melted, but even these products consisted of only Sm_5Ge_4-type phases.

Triels: La_5Ge_3Z compositions for $Z =$ Al, Ga, or In within Ta containers were heated in a high temperature furnace. The Al reactions resulted in complex mixtures that appeared to contain an Mn_5Si_3-type phase as well as $LaAl_2Ge_2$ (anti-La_2O_3) [17] and unknown phases. Further studies were limited to LaAlGe and related phases [18]. Results with Ga and In are summarized in Table 1. Slow cooling was required to obtain good single crystals. Guinier powder diffraction patterns of the two products were very similar, and each could be indexed to an orthorhombic cell of the nominal Sm_5Ge_4-type. However, the relative intensities of some lines clearly differed from those for an Sm_5Ge_4-type model, particu-

larly for the [132] and [231] reflections. Furthermore, the b/a and b/c axial ratios of the compounds were larger than those of the corresponding La_5Ge_4 and other known Sm_5Ge_4-type compounds. This problem was solved via a single crystal diffraction study of La_5Ge_3Ga; adequate crystals of the indium phase were not obtained.

Structural studies, β-La_5Ge_3Si: The single crystal structural investigation of the high temperature β-form of nominal La_5Ge_3Si crystals that grew following arc melting proceeded in the usual manner with the aid of a CAD4 diffractometer and SDP software [19]. Redundant data sets were collected after 25 reflections from the program SEARCH had been indexed with a tetragonal cell. Data preparation included absorption corrections according to three psi-scans, Lorentz and polarization corrections, and averaging in the Laue symmetry $P4/mmm$. Precession and Laue cone photographs taken with long exposures confirmed the Laue symmetry $4/mmm$. Careful inspection of the reflection data and higher-level precession photos indicated systematic reflection conditions $00l$; $l = 4n$ and $0k0$; $k = 2n$. These correspond to the possible acentric space groups $P4_12_12$ and $P4_32_12$, and the former proved to be correct during refinement.

The structure was refined from an initial direct methods model (SHELXS [20]). Since Si and Ge sites could not be distinguished, all nonmetal peaks were initially assigned to germanium. The weighting was according to the counting statistics. Isotropic refinement resulted in large thermal parameters for the pure germanium sites, and the final refined occupancies for two of the nonmetal positions at this stage were essentially equal, 86.5(2)% and 86.9(2)% for Ge1 and Ge2, respectively. These correspond to mixtures of 78.0(3)% Ge, 22.0(3)% Si for Ge1, and 78.6(3)% Ge, 21.4(3)% Si for Ge2 assuming full occupancy of each. Anisotropic refinement after application of DIFABS [21] resulted in final residuals of $R = 2.4\%$; $R_w = 3.0\%$. These give the refined stoichiometry $La_5Ge_{3.13(1)}Si_{0.87(1)}$, close to the loaded stoichiometry of La_5Ge_3Si. (Since the crystals grew from an arc-melted button during solidification, some fractionation may have occurred.) The largest peak in the final difference Fourier map was $1.3\,e^-/\text{Å}^3$, 2.1 Å from Ge1. Summaries of single crystal and structure solution data for β-La_5Ge_3Si (Zr_5Si_4 type) are presented in Tables 2–4.

La_5Ge_3Ga: In hopes of a better understanding of the triel derivatives, especially the errant intensities of certain nominal Sm_5Ge_4 reflections, single crystals of La_5Ge_3Ga were isolated and investigated using the AFC6R Rigaku diffractometer and TEXSAN [22] crystallographic software. A four-fold redundant data set $(h, \pm k, \pm l)$ up to $2\theta_{max} = 55°$ was collected after an orthorhombic cell was indicated by the indexing of 25 reflections. Axial photos confirmed the presence of

mirror planes perpendicular to the each axes, indicating a Laue symmetry *mmm*. Following data averaging in the corresponding Laue class, inspection of the reflection data and axial photos indicated reflection conditions that corresponded to those of either space group *Pnma* or *Pn2$_1$a*. Refinement proved the former to be correct. The data were then transformed to the standard setting, and the refinement proceeded in the usual manner. Other important crystal and refinement data for La$_5$Ge$_3$Ga are listed in Table 5.

Since the lattice parameters were similar to those found for Sm$_5$Ge$_4$ and the possible space groups were the same, an initial attempt was to fit the observed structure factors to atomic parameters based on those of Sm$_5$Ge$_4$. However, isotropic refinements with this model resulted in unsatisfactory residuals, $R = 20\%$,

$R_w = 24\%$, even when occupancies were allowed to vary. Direct methods (SHELXS) were then employed to provide a better starting model. Also, since X-ray methods cannot readily distinguish Ge from Ga, all peaks were assigned to Ge, and the rough model was refined toward completion via standard full-matrix calculations and Fourier syntheses. Absorption effects were corrected with the aid of three psi-scans and a subsequent application of DIFABS after isotropic refinement. The process proceeded satisfactorily and gave final residuals of $R = 3.3\%$, $R_w = 3.6\%$, well-behaved thermal parameters, and satisfactory esd's. Occupancies were refined keeping La1 at the ideal value, and this resulted in 100.0(1)%, 100.2(2)%, 99.2(3)%, 97.6(4) and 99.8(3)%, occupancies for La2, La3, Ge1, Ge2, and Ge3, respectively. The overall refined stoichiometry is La$_5$Ge$_{3.96(1)}$, although statistically all but Ge1 gave essentially ideal values. In terms of atomic numbers, the overall Ge occupancies are indistinguishable from La$_5$Ge$_3$Ga (= La$_5$Ge$_{3+(31/32)}$ = La$_5$Ge$_{3.97}$ for neutral atoms). This agreement strongly supports the presence of Ga, probably on the Ge1 site. More important was the subsequent synthesis of a single-phase product ($>95\%$) from the loaded stoichiometry La$_5$Ge$_3$Ga, an excellent proof of composition. The final difference Fourier was essentially flat with the largest residual peak of $1.67\,e^-/Å^3$ close to La2. The final positional and thermal parameters as well as important distances and angles for the Gd$_5$Si$_4$-type result are listed in Tables 6 and 7, respectively. All structural data are reported in the TIDY-selected settings [23].

3. Results and discussion

Our previous work on the solid-state chemistry of La$_5$Ge$_3$Z phases based on an Mn$_5$Si$_3$ host structure showed a wide and flexible interstitial chemistry [1,13]. This has since been elaborated [24]. The interstitial

Table 2
Data collection and refinement parameters for β-La$_5$Ge$_3$Si

Space group, Z	$P4_12_12$ (No. 92), 4
Cell param^a (Å, Å^3)	
a	8.148(1)
c	15.294(2)
V	1051.4(4)
Crystal dimension	$0.06 \times 0.06 \times 0.10$ mm
Diffractometer	Enraf–Nonius CAD4
$2\theta_{max}$	65°
Collected octants	$h, \pm k, \pm l$
Absorp. coeff. (cm^{-1}, Mo$K\alpha$)	322.4
Reflections	
Measured	7783
Observed ($>3\sigma_I$)	6690
Independent	885
R_{ave} (obs.)	3.1%
No. of param. refined	46
R	2.4%
R_w	3.0%
Largest param. shift	0.01
Secondary extinction coeff., 10^{-5}	1.93(6)
Largest residual peak	$1.3\,e^-/Å^3$

^{a}Guinier data with Si as an internal standard, 22 °C.

Table 3
Refined lattice and displacement ellipsoid parameters for β-La$_5$Ge$_3$Si

Atom	x	y		z	Occup. Ge/Si	
La1	0.13199(5)	0.49086(5)		0.45482(3)		
La2	0.13562(5)	0.01450(5)		0.37516(4)		
La3	0.18565(6)	x		0		
Ge1	0.2932(1)	0.0655(1)		0.18881(7)	0.780(3)/0.220(3)	
Ge2	0.3409(1)	0.3007(1)		0.30809(6)	0.786(3)/0.214(3)	
Atom	B_{ll}	B_{22}	B_{33}	B_{12}	B_{13}	B_{23}
La1	0.67(1)	0.73(1)	0.76(1)	0.05(1)	−0.11(1)	−0.16(1)
La2	0.65(1)	0.63(1)	0.59(1)	0.02(1)	−0.07(1)	−0.12(1)
La3	0.84(1)	B_{11}	0.77(2)	−0.02(2)	−0.09(1)	$-B_{13}$
Ge1	0.89(3)	0.85(3)	0.68(3)	−0.09(3)	−0.05(3)	0.04(3)
Ge2	0.76(3)	0.60(3)	1.04(3)	−0.20(3)	0.14(4)	−0.16(3)

Table 4
Important interatomic distances (Å) and angles (deg) in β-La$_5$Ge$_3$Si

Atom–atom	Distance
La1–La3 × 2	3.7581(6)
La2–La3 × 2	3.6273(5)
La2–La3 × 2	3.6006(5)
La3–La3 × 2	3.758(1)
La3–La3 × 2	3.7594(6)
La3–La3 × 2	3.758(1)
La1–Ge1	3.242(1)
La1–Ge1	3.493(1)
La1–Ge1	3.237(1)
La1–Ge2	3.215(1)
La1–Ge2	3.306(1)
La1–Ge2	3.363(1)
La2–Ge1	3.153(1)
La2–Ge1	3.151(1)
La2–Ge1	3.183(1)
La2–Ge2	3.048(1)
La2–Ge2	3.178(2)
La2–Ge2	3.013(1)
La2–Ge2 × 2	3.267(1)
La3–Ge1 × 2	3.238(1)
La3–Ge2 × 2	3.267(1)
Ge1–Ge2	2.674(1)

Interatomic angles

Atom–atom–atom	Angle
Ge1–La1–Ge1	31.99(1)
Ge1–La1–Ge1	92.95(6)
Ge1–La1–Ge1	137.48(2)
La3–La1–La3	97.32(1)
La1–La3–La1	177.85(2)
La1–La3–La1	114.16(2)
La1–La3–La1	178.97(2)
La1–La3–La1	65.86(1)
La3–La2–La3	103.72(2)
Ge1–La1–Ge1	172.61(2)
Ge1–La2–Ge2	142.16(2)
Ge2–La2–Ge2	93.11
Ge1–La3–Ge1	90.89(1)
Ge1–La3–Ge2	88.26(1)
Ge2–La3–Ge2	86.95(1)
Ge1–La3–Ge1	92.27(1)
Ge1–La3–Ge2	178.75(2)
Ge1–La3–Ge1	177.38(2)
Ge1–La3–Ge2	89.84(1)
La3–Ge1–Ge2	116.10(2)
La3–Ge2–Ge1	119.53(2)

Table 5
Data collection and refinement parameters for La$_5$Ge$_3$Ga

Space group, Z	$Pnma$ (No. 62), 4
Crystal dimens., mm	$0.08 \times 0.08 \times 0.12$
Diffractometer	Rigaku AFC6R
Cell parameters[a] (Å, Å^3)	
a	7.910(1)
b	15.294(2)
c	8.252(1)
V	1021.9(5)
$2\theta_{max}$	55°
Collected octants	$h, \pm k, \pm l$
Absorption coeff. (cm^{-1}, Mo$K\alpha$)	316.0
Reflections	
Measured	5036
Observed ($>3\sigma_I$)	3594
Independent	981
R_{ave}, all data	13.4%
No. of parameters	50
R	3.3%
R_w	3.6%
Largest parameter shift	0.00
Secondary extinct. coeff. (10^{-8})	5.3(3)
Largest residual peak, e$^-$/Å^3	1.7

[a] Guinier film data with Si as an internal standard, 22 °C.

chemistry of the host La$_5$Ge$_3$ appears to be dominated by size and electronic effects. Parallel to these synthesis experiments, the syntheses of other La$_5$Ge$_3$Z compounds with Z = Si, Sn, Pb, Ga and In were pursued in which the diminished electron counts available with fully stoichiometric Z favor dimerization among the main group elements. Our results from these experiments are summarized in Table 1. One interest was to understand the three structure types that are assumed by many 5:4 rare-earth-metal tetrelides and, if possible, to

rationalize their structure and bonding using Zintl–Klemm concepts.

La$_5$Ge$_3$Si: The syntheses of three structurally different compounds in the stoichiometry range La$_5$Ge$_3$Si$_x$, $0.7 < x < 1.0$, provides interesting structure and bonding considerations. Arc-melting of the La$_5$Ge$_3$Si$_{0.75}$ composition gave a single-phase product with the well-known Mn$_5$Si$_3$Z-type structure. This well studied structure was not detailed, but it is not that of the substoichiometric superstructure La$_{15}$Ge$_9$Z [13]. However, annealing this at 1000–1200 °C resulted in disproportionation into the corresponding La$_5$Ge$_3$ (Mn$_5$Si$_3$), with probably little Si content, and α-La$_5$Ge$_3$Si with an Sm$_5$Ge$_4$-type structure. A lower Si content resulted only in lesser amounts of the latter. However, arc melting of La$_5$Ge$_3$Si$_x$ compositions for $x > 0.75$ yielded mixtures of the limiting Mn$_5$Si$_3$-type phase La$_5$Ge$_3$Si$_{0.75}$ and, with increasing x, increased amounts of tetragonal β-La$_5$Ge$_3$Si. The contrast with the La$_5$Ge$_{3+x}$ system is noteworthy in that only the $x \sim 0$ phase with the Mn$_5$Si$_3$ structure is stable there, without an additional stoichiometry range via self-interstitials [1].

Structure of β-La$_5$Ge$_3$Si: This is isotypic with the tetragonal Zr$_5$Si$_4$ structure type ($P4_12_12$, Section 2, Tables 3, 4) [3]. The structure type has evidently not been satisfactorily described before [25], but it is generally classified as one with only dimeric (dumbbell) anions. In the present case, the single type of dimer has a random $\sim$25% Si and an interatomic distance of 2.675(1) Å, which can be compared with the Si–Si bond

Table 6
Refined parameters for La$_5$Ge$_3$Ga

Atom	x	y	z	Occupancy	
La1	0.02506(7)	0.59580(4)	0.18348(7)	1.0	
La2	0.31675(7)	0.12129(4)	0.17699(7)	1.0	
La3	0.1504(1)	0.25	0.51630(1)	1.0	
Ge1	0.1501(1)	0.04055(7)	0.4709(1)	0.992(3)[a]	
Ge2	0.0224(1)	0.25	0.1031(1)	0.976(4)[a]	
Ge3	0.2612(1)	0.25	0.8757(1)	0.998(3)[a]	
Atom	U_{11}	U_{22}	U_{33}	U_{12}	U_{13}	U_{23}
La1	0.0157(3)	0.0148(3)	0.0130(3)	−0.0031(2)	0.0021(2)	0.0020(2)
La2	0.0147(3)	0.0099(3)	0.0112(3)	0.0000(2)	−0.0014(2)	0.0004(2)
La3	0.0205(4)	0.0138(4)	0.0169(4)	0.0	−0.0012(3)	0.0
Ge1	0.0185(6)	0.0119(6)	0.0125(6)	−0.0017(4)	−0.0011(4)	−0.0021(4)
Ge2	0.0138(8)	0.0122(8)	0.0163(8)	0.0	0.0032(6)	0.0
Ge3	0.0186(6)	0.0136(6)	0.0137(6)	0.0	0.0010(4)	0.0

[a]Refined as Ge.

Table 7
Important interatomic distances (Å) and angles (deg) in La$_5$Ge$_3$Ga

Atom–atom	Distance
La1–La3 × 2	3.691(1)
La1–La3 × 2	3.749(1)
La1–Ge1	3.309(1)
La1–Ge1	3.224(1)
La1–Ge1	3.281(1)
La1–Ge2	3.361(2)
La1–Ge3	3.306(1)
La1–Ge3	3.307(1)
La2–La3	3.658(1)
La2–La3	3.667(1)
La2–Ge1	3.015(1)
La2–Ge1	3.024(1)
La2–Ge1	3.157(1)
La2–Ge2	3.133(1)
La2–Ge2	3.109(1)
La2–Ge3	3.201(1)
La3–Ge1 × 2	3.225(1)
La3–Ge2	3.557(2)
La3–Ge2	3.103(2)
La3–Ge3	3.205(1)
La3–Ge3	3.093(1)
Ge1–Ge1	2.722(2)
Ge3–Ge2(Ga)	2.663(2)

Interatomic angles

Atom–atom–atom	Angle
La2–La3–La2	65.10(2)
La2–La3–La2	102.40(2)
La1–La3–La1	114.35(2)
La1–La3–La1	77.96(2)
Ge2–La1–Ge2	89.62(4)
Ge2–La1–Ge3	89.62(4)
Ge2–La2–Ge3	177.63(5)
Ge3–La3–Ge3	90.32(2)
Ge1–La3–Ge3	91.81(2)
Ge1–La3–Ge1	166.66(4)
Ge2–La3–Ge2	88.02(3)
Ge3–La3–Ge2	177.63(5)
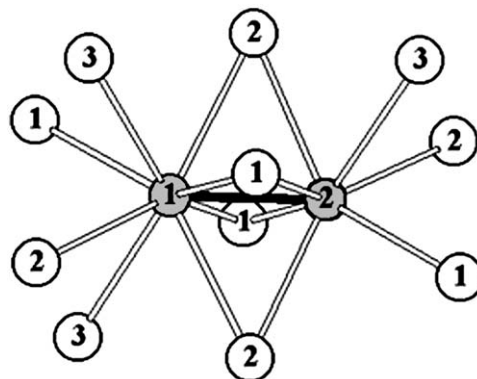
Fig. 1. The distorted confacial, square antiprismatic configurations La$_{11}$Tt$_2$ about the tetrelide dimer in β-La$_5$Ge$_3$Si (Zr$_5$Si$_4$-type, $P4_12_12$, Tt = Ge,Si). Open circles are La, gray circles are tetrel.

distance of 2.30 Å in U$_3$Si$_2$ [26] and a much closer 2.658 Å in the Ge–Ge dimer in Sm$_5$Ge$_4$ [5]. The Pauling single bond distances [27] for Si and Ge are 2.34 and 2.48 Å, respectively, but charges on the anions and π electron repulsions often distort such simple measures.

The Zr$_5$Si$_3$ structure and other types have been described as derived from the more symmetric parent U$_3$Si$_2$ structure ($P4/mbm$). This contains formal Si$_2^{-6}$ dumbbells in U$_{12}$Si$_2$ building units in the form of pairs of Si-centered square antiprisms sharing a common square face, as previously alluded to by Karpinskii and Evseev [28]. However, in the present structure type the $M_{12}Tt_2$ analogue is further distorted from an ideal antiprismatic coordination with the loss of one metal atom to form La$_{11}Tt_2$ fragments, as shown in Fig. 1 for La$_5$Ge$_3$Si. These units are in turn tetrahedrally close-packed [29] along the 4-fold screw axis with the lanthanum atoms as common vertices, viz., (La$_{4/4}$ + La$_{4/4}$ + La$_{3/6}$)Tt_2, to yield the stoichiometry La$_5Tt_4$. But

this approach is not as useful and as general as other comparisons.

Zr_5Si_4– Sm_5Ge_4-type relationships: We begin with the relationship between the α-(Sm_5Ge_4-type) and β-(Zr_5Si_4-type) forms of La_5Ge_3Si. One clear difference is the number of dimers per formula unit, the former in a layered structure with one dimer (plus two monomers) and the latter a three-dimensional network with two types of dimers. The two space groups, $Pnma$ and $P4_12_12$, respectively, do not represent a group–subgroup relationship. However, the lattice parameters of the orthorhombic α-phase suggest a possible pseudo-tetragonal cell with b as the unique axis (Table 1). Although both structures are related to the U_3Si_2 structure type, a detailed inspection does not immediately reveal any close relationships between the two. The dimers in the α-phase lie in the basal plane of the layers, perpendicular to the pseudo-tetragonal (b) axis, whereas those in the β-phase are tilted toward the tetragonal axis.

To better understand their similarities and differences, we start with a common structural unit—an La3-centered La_8 cube (of La1 and La2) in β-La_5Ga_3Si (Zr_5Si_4 type) that is capped on all faces with Ge(Si) to give the $La(La)_8Ge_6 = La_9Ge_6$ unit shown in Fig. 2. (The Si component appears to be completely disordered to X-rays.) All three La have six Ge neighbors, but this unit is smaller, nearly octahedral and with only eight La neighbors as well. This can alternatively be described as an octahedral coordination polyhedron of six Ge(Si) atoms about La3 (hatched) on which the eight triangular faces are capped by La. There are four Ge(Si)1 and two Ge(Si)2 atoms in this unit, and every La atom in the cube is shared by another La_9Ge_6 unit to yield the observed stoichiometry $La(La_{8/2})(Ge1)_{4/2}(Ge2)_2 = La_5Ge_4$. This unit is also present, albeit slightly distorted, in Sm_5Ge_4-type structures (below). The
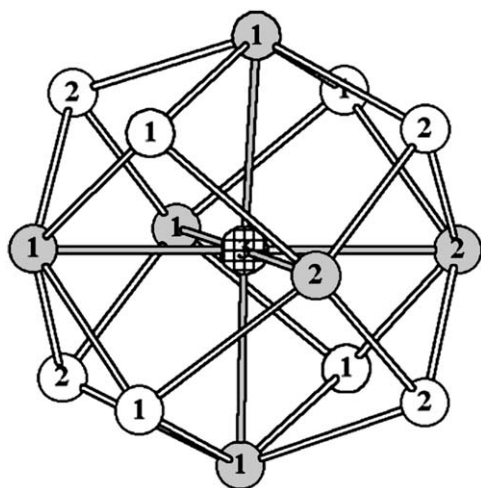
complex connectivity between dimers of $La_9(Ge,Si)_6$ in the tetragonal structure is shown in two views in Fig. 3. These units are twisted with respect to their pseudo-octahedral axes and then fused to share La1, La2 and Ge1 vertices. In addition, Ge1 and Ge2 atoms in adjacent units form the Ge1–Ge2 dimer. The construction in Fig. 3(a), which will also become familiar among the other 5–4 compounds considered, is viewed here normal to a horizontal La3–La3 interconnection, but this lies at odd angles to the cell axes (46° to a, 11° to b, 48° to c). Fig. 3(b) shows the same group in a [100] projection with the c-axis vertical. This highlights the complexity of the Zr_5Si_4-type bonding between four layers that lie normal to c along the 4_1 axis compared with the other 5–4 structure types that follow. A parallel projection of one layer in this structure around the organizing La3 (hatched) atoms is shown in a [100] view around $z = 0$ in Fig. 4(a), the width and depth of the
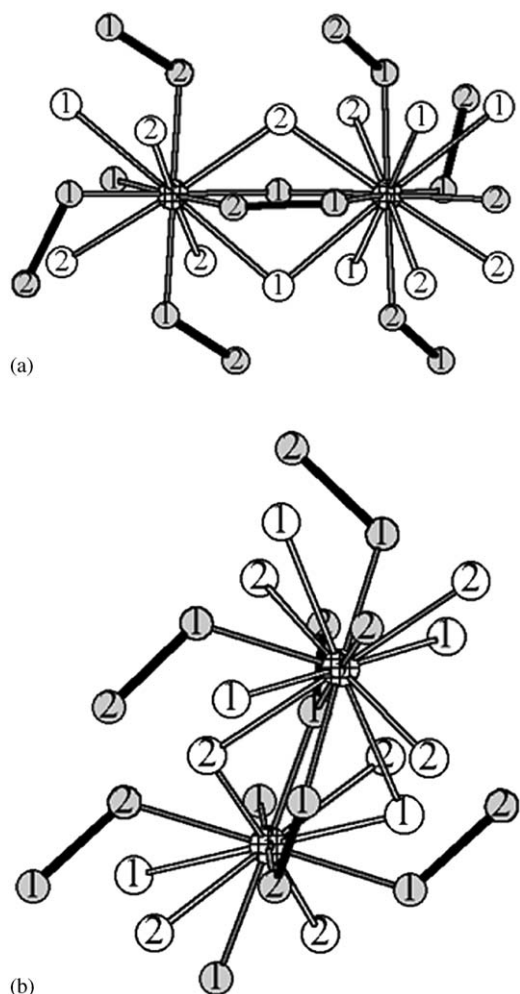

(a)

(b)

Fig. 3. Bonding between pairs of $La(3)(Ge)_6(La_8)$ units in (Fig. 2) in β-La_5Ge_3Si with the formation of Ge(1)–Ge(2) bonds (black): (a) The unit is viewed normal to a horizontal La(3)–La(3) axis. (b) A [100] view of the same $(La(3)Ge_6La)_2$ units with $\vec{c}$ vertical. The layers in La_5Ge_3Si run horizontally in this view.

Fig. 2. The La_9Tt_6 building block. The La(3)–Ge6 octahedron with face-capping La1,2 atoms (white) in β-La_5Ge_3Si. La3 is hatched, the Ge atoms are gray, and La(3)–Ge contacts are gray.
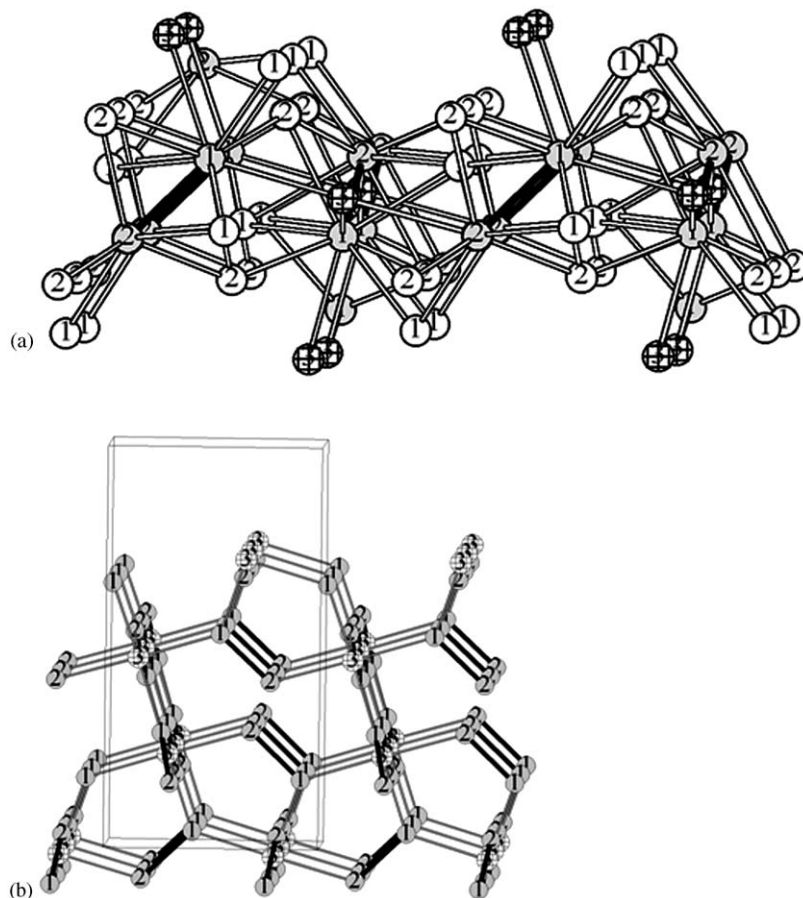
Fig. 4. (a) [100] View of one of the four layers normal to ADVANCE $\vec{c}$ that contain all dimeric Tt_2 units in β-La$_5$Ge$_3$Si ($P4_12_12$). The area shown is around $z \sim 0$ and is roughly $2a \times 2b$. Tt atoms are gray and the Tt_2 bonds are black. (b) A larger [100] (view $\vec{c}$ vertical) of only the La(3) and Tt (gray) atoms, the Tt_2 dimers (black), and all nominal La(3)–Ge bonds (gray) in β-La$_5$Ge$_3$Si.

view being $2a$ and $2b$. Note that all dimers lie within the layer, and their tilts along the view direction alternate appreciably. The interlayer connection of the dimer units, Fig. 3(b), spans the gaps between layer sections in Fig. 4(a), the interlayer midpoint in the former lying near the La1 layers in the earlier view but with the unit tilted enough that one La3 center is out of this section. Fig. 4(b) emphasizes just the Ge–Ge and La3–Ge bonded network in and between three layers (below). These all reflect the action of the 4_1 axes along, e.g., 0, 1/2, z, that lead to tetrahedrally close-packed strings and a three-dimensional network of La$_9$(Ge,Si)$_6$ units. Tetrahedral packing of structural units is often used to rationalize and differentiate many intermetallic structures, and it conforms to the Frank–Kasper rules [29].

The structure of α-La$_5$Ge$_3$Si (Sm$_5$Ge$_4$-type) structure can be simply expressed in terms of a different packing of basically the same La$_9$Ge$_6$ units, which is illustrated in Fig. 5 with the central La1 (hatched) according to recent data for the isotypic La$_5$Ge$_4$ [30]. In comparison with Fig. 3, the Ge1 atom tilt ($\angle$ Ge3–La1–Ge3 = 169.4°) from the pseudo-tetragonal axis (b) in this structure
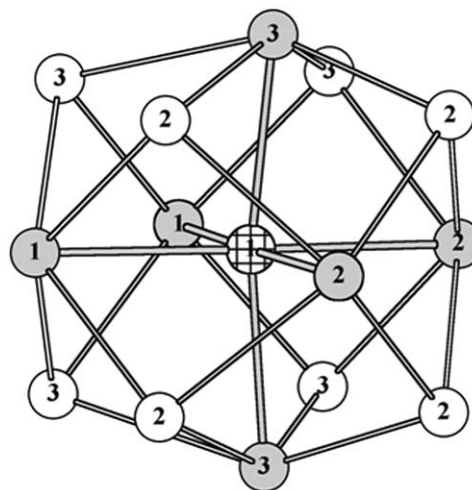

Fig. 5. The Ge$_6$La$_8$ cube octahedra around the centering La(1) (hatched) in La$_5$Ge$_4$ (Sm$_5$Ge$_4$ type, $Pnma$).

effectively lowers the local symmetry ($4/m \Rightarrow mmm$) at the central atom. In the α-structure, the La$_9$(Ge,Si)$_6$ units are linked parallel to the a–c plane into layers, in

contrast to the three dimensional packing of $La_9(GeSi)_6$ units seen above, but leaving "dangling" Ge3 atoms between the layers. (The Si portion probably is favored at the Ge1, Ge2 sites because of stronger Si–Si bonding.) Now each La_9Ge_6 "cluster" is connected to four other units. The stepwise connections between La_9Ge_6 units is shown in Figs. 6 and 7. In the first step, two units share two La3 and one Ge1 atoms as common vertices, which also lead to the formation of bridging (Ge1–Ge2) dimers from Ge atoms on adjoining La_9Ge_6 units. This is very similar to the connectivity found in β-La_5Ge_3Si (Fig. 3(a)), but the lack of twisting leads to layers as shown in an extended view in Fig. 7 and dangling Ge3 atoms. The twisting of La_9Ge_6 units observed in high-temperature β-La_5Ge_3Si affords a more efficient tetrahedral close
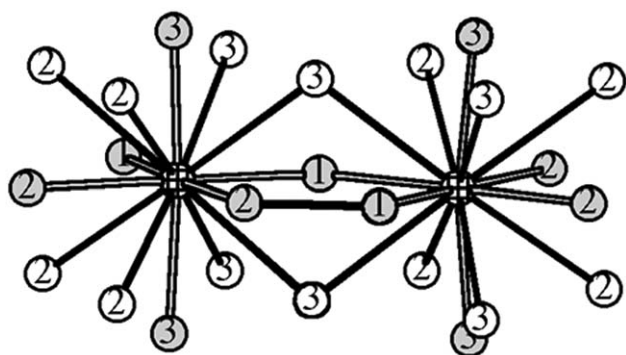
Fig. 6. Bonding between pairs of La(1)-centered polyhedra and the Ge_2 dimer generation in La_5Ge_4. The Ge(3) atoms at top and bottom remain unbonded to each other.
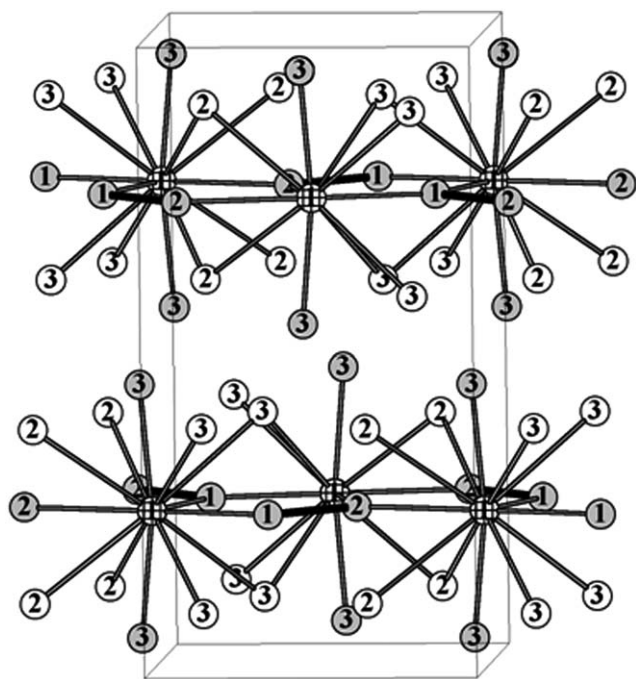

Fig. 7. [100] view of the Sm_5Ge_4-type (Pnma) structure of La_5Ge_4 and α-La_5Ge_3Si; $\vec{b}$ is vertical.

packing of these units, with a smaller tetragonal cell volume (at the 2.7σ level neglecting any possible Si deficiency, Table 1) and a higher density for the metastable β-form at room temperature. (The formation of the higher density polytype β-La_5Ge_3Si with more bonding but higher symmetry at a higher temperature does seem a little unusual but not impossible.) The connectivity of La_9Ge_6 units in La_5Ge_4 (α-La_5Ge_3Si) results in layers built of what can be described as prisms or fused square antiprismatic units of La around the Ge_2 dimers. The more regular atom coordination around neighboring Ge3 atoms amounts to slightly distorted bicapped trigonal prisms that a share rectangular square faces, in contrast to Fig. 1. The distance between the nearest unbonded Ge3 atoms across the gap in La_5Ge_4 is quite long, 3.90 Å. A similar but less detailed description of the above interrelationship has been given by Rodewald et al. for tetrelide examples with mixed rare-earth metals [31].

Since the silicide La_5Si_4 also exists in the Zr_5Si_4-type structure [32], it is possible that tetragonal (β) La_5Ge_3Si is part of a high-temperature homogeneity range within the $La_5Si_{4-x}Ge_x$ system. This is supported by the subsequent arc-melting syntheses of single-phase tetragonal products $La_5Ge_{2.5}Si_{1.5}$ and $La_5Ge_{2.0}Si_{2.0}$. However, the limits of the homogeneity range were not determined, and the range over which the Sm_5Ge_4-type of $La_5Ge_{4-x}Si_x$ exists at lower temperature remains an open question. However, annealing of the above Si-richer compositions at 1100 °C did not result in any transformation into the Sm_5Ge_4-type, contrary to what is observed for La_5Ge_3Si. Furthermore, the structural relationships between the La_5Ge_3Si structures indicate that this transformation is best described as first order. These observations are consistent with studies by Gschneidner and coworkers [33] that show that the tetragonal Zr_5Si_4 structure of $La_5Si_{4-x}Ge_x$ samples persists for $x > 0.75$, but a Sm_5Ge_4-type structure occurs for $x < 0.50$.

La_5Ge_3Sn and La_5Ge_3Pb: The $La_5Ge_3Si_x$ results provided an incentive to synthesize the tin Sn and Pb analogues, and these efforts demonstrated that La_5Ge_3Sn and La_5Ge_3Pb both exist only in the Sm_5Ge_4 structure, even with rapid quenching (Table 1). The absence of a tetragonal β-La_5Ge_3Si (Zr_5Si_4)-type phase for these might be ascribed to the larger sizes of Sn and Pb which generate larger interatomic distances between the tetrelides and the cations as well as between tetrelide atoms (matrix effects). This would make the more efficient tetrahedral packing found in β-La_5Ge_3Si unfavorable. An additional aspect is that the binaries La_5Ge_4, La_5Sn_4 [34], and La_5Pb_4 [35] all crystallize in an Sm_5Ge_4 structure, so that La_5Ge_3Sn and La_5Ge_3Pb may only be parts of a wider solubility range between these 5–4 phases which also extends partially in the other way, as with La_5Ge_3Si (at low temperature).

Triels: The results of the experiments involving silicon also led us to investigate the reactions of La_5Ge_3 with the group 13 elements Al, Ga, In. Simple electron counting indicates that any La_5Ge_3Ga, La_5Ge_3In or La_5Ge_3Al product with an Sm_5Ge_4 structure would be closed shell Zintl phase *if* classic dimeric anions with 10-valence-electrons were retained. Present knowledge suggests that this is quite unlikely (see below).

Reactions of La_5Ge_3 with Al resulted in products with complicated powder diffraction patterns (see Section 2). The synthetic reactions with Ga and In led to the isostructural La_5Ge_3Ga and La_5Ge_3In. Differences in the relative intensities of the [132] and [231] lines (Section 2) aided in differentiating this all-dimer Gd_5Si_4-type structure (below) from the single dimer Sm_5Ge_4 and Eu_5As_4-types, even though all occur in the same space group. Efforts to grow single crystals of La_5Ge_3In by prolonged reactions failed, although further investigations of the ternary system La–In–Ge resulted in the syntheses of two other metal-rich compounds, La_3In_4Ge and La_3InGe [14].

Structure of La_5Ge_3Ga: The structure of La_5Ge_3Ga is of the parent Gd_5Si_4-type (Tables 6 and 7), which is also the case for several relevant mixed cation pnictide salts, the recently reported $Na_2Ba_3Sb_4$ [36][3] and $K_2Ba_3Sb_4$ [37] as well as the earlier analogues $Na_2M_3Pn_4$, $M =$ Eu, Sr, $Pn =$ P, As studied by von Schnering and coworkers [38,39]. All contain only main group element dimers and occur in the same space group as Sm_5Ge_4 types, *Pnma*. The last group of five are all conceptually generated by means of two-electron oxidations of the monoanions in $(Ae^{2+})_4 Pn_2^{4-}(Pn^{3-})_2$ substrates (Sm_5Ge_4 or Eu_5As_4-type) through substitution of two Na^+ or K^+ for two A^{2+}. The gallium result arises by a different mode, a one-electron oxidation ($Ge \Rightarrow Ga$) of, in the ideal Zintl phase description, Ge^{4-} in $(La^{3+})_5 (Ge_2^{6-})(Ge^{4-})_2 (e^-)$ (Sm_5Ge_4-type) to give $(La^{3+})_5 (Ge_2^{6-})(GeGa^{7-})(e^-)_2$ (Gd_5Si_4-type), the extra "free" electrons in both of these descriptions being characteristic of such tetrelide phases (see below).

The structure of La_5Ge_3Ga is qualitatively closely related to the Sm_5Ge_4 type, as represented by α-La_5Ge_3Si or La_5Ge_4. Both are characterized by the same layered connectivity of La_9Ge_6 units along the a–c plane, but interlayer displacements now lead to the dimerization of all the Ge positions to give two dimer distances, 2.663(2) Å for Ge2–Ge3 and 2.722 (2) Å for Ge1–Ge1 (between layers). Occupancy refinements for a rather marginal situation (see Section 2) suggest Ga may lie mainly on the Ge2 site. The Pauling single bond values for homoatomic bonds are 2.53 and 2.50 A for 4-bonded Ga and Ge, respectively [27] but longer distances in such dimers are generally observed and

attributed to higher electron populations on the atoms, charge repulsion within the dimer, and to packing effects with larger atoms. A further comparison of the atomic positions in La_5Ge_3Ga vs. those in Gd_5Si_4 [40] clearly demonstrate the similarity, there being no significant differences in fractional coordinates ($\leqslant 0.006$ or 0.05 Å). The La_5Ge_3Ga structure can be described in the same manner as that used to differentiate Zr_5Si_4 and Sm_5Ge_4. This allows us to trace how the additional dimer in La_5Ge_3Ga evolves from the Sm_5Ge_4-type structure by simpler interlayer translations.

We begin with the same La3-centered La_9Tt_6 building unit as shown in Fig. 8. Comparison of this with those found in Zr_5Si_4 and Sm_5Ge_4 (β-La_5Ge_3Si) (Figs. 2, 5) show subtle yet crucial differences. The Ge1–La3–Ge1 angular distortion in La_5Ge_3Ga is largest among the three structures, 166.66(4)° vs. 169.4° in La_5Ge_4 and 177.38(2)° in β-La_5Ge_3Si. The interatomic distances between the central La3 and its surrounding neighbors are less symmetrical in La_5Ge_3Ga, which is also reflected in the axial ratios of the different unit cells, b/c especially in La_5Ge_4 (1.894) vs. La_5Ge_3Ga (1.853). In La_5Ge_3Ga, each La_9Tt_6 unit is linked to four other units to give layers in the same manner as in La_5Ge_4 (Sm_5Ge_4), starting with the dimeric center, Fig. 9. In fact, Wang et al. [6] in describing Gd_5Si_4 state that it and Sm_5Ge_4 have identical "tilting patterns". But the stacking of the layers formed from interconnected La_9Ge_6 units in orthorhombic La_5Ge_3Ga includes interlayer slippage and yields a second type of dimers rather than the dangling Ge1 monomers that are present in two adjacent layers in α-La_5Ge_3Si, Fig. 7. The present result is shown in Fig. 10. The coordination of the added Ge1 dimers is by a pair of more regular bicapped trigonal prisms that share a common square face,
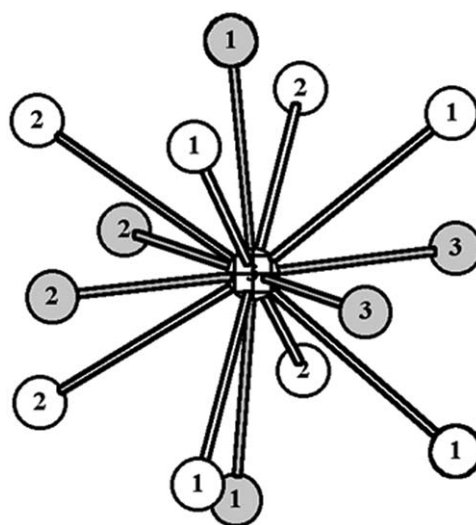

Fig. 8. [100] View of the La(3)-centered La_9Tt_6 unit in La_5Ge_3Ga (Gd_5Si_4) with Tt atoms gray, La white, and La(3)–Tt bonds gray. $\vec{b}$ vertical.

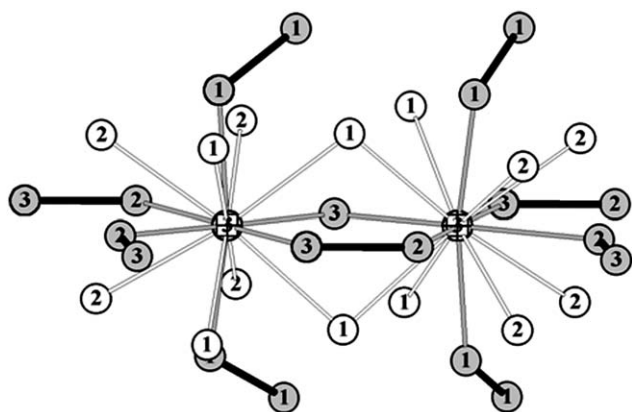[3]The y coordinate of Sb3 in $Na_2Ba_3Sb_4$, 0.0363(1), was incorrect in the earlier publication.

Fig. 9. Bridging of two La_9Tt_6 units in La_5Ge_3Ga (~[101]) plus all surrounding dimers.

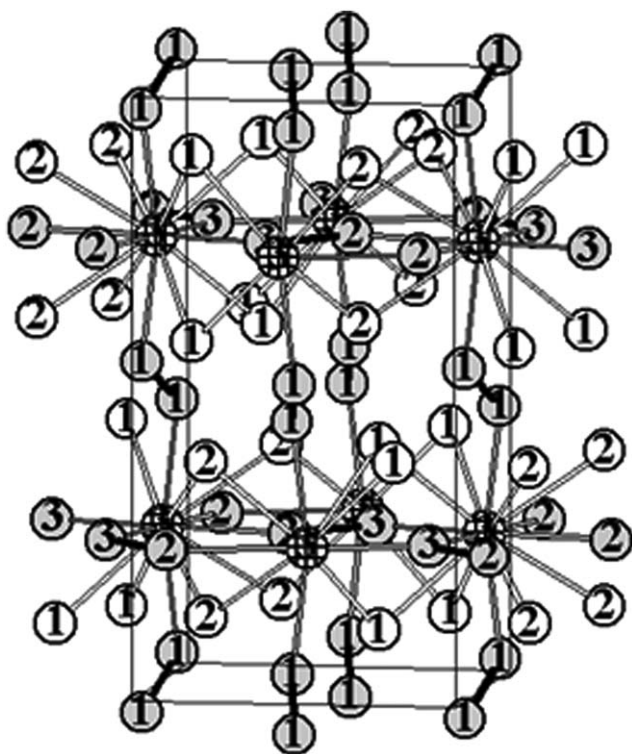Fig. 11. The environment of the interlayer Ge(1)–Ge(1) dimers between La(3) units in La_5Ge_3Ga (Gd_5Si_4).

Fig. 10. ~[100] view of the La_5Ge_3Ga (Gd_5Si_4) structure with the cell marked ($\vec{b}$ vertical) (*Pnma*).

Fig. 11, in contrast to the corresponding fragment in α-La_5Ge_3Si (Fig. 1). The dimer formation can be correlated with the "tilting" displacement of the Ge1 atoms from the *c*-axis of the La_9Ge_6 unit coupled with the displacement of La2 atoms to "open up" the common square face. Likewise, the dimerization of Ge1 atoms can be related to the increased distance between Ge1 and the central La3 of the La_9Ge_6 unit, 3.18 Å in La_5Ge_4, and 3.22 Å in La_5Ge_3Ga. The increased axial La3–Ge1 distances also correlates with the increased *b*/*a* axial ratio of La_5Ge_3Ga with respect to the value in La_5Ge_4, 1.934 vs. 1.919. It is also
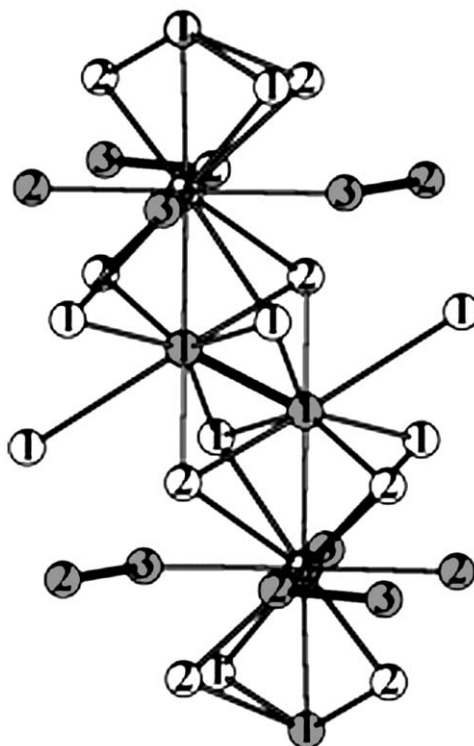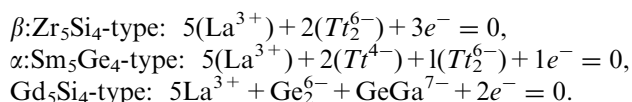
important to note that the dimer distances in La_5Ge_3Ga, 2.663(2) and 2.722(2) Å, are significantly shorter than the single one in La_5Ge_4, 2.77 Å [30], presumably because fewer antibonding states on the dimers as occupied (below).

The substitution of one gallium for germanium in Gd_5Ge_4 likewise changes the Sm_5Ge_4 structure of the former into the Gd_5Si_4 analogue [41]. These transitions become especially interesting in certain Gd_5Tt_4 systems. The "zippering" transformation between Sm_5Ge_4 and Gd_5Si_4-type interlayer bonding in $Gd_5Si_{4-x}Ge_x$ also contains a half-zippered monoclinic structure between $Gd_5Si_2Ge_2$ and Gd_5SiGe_3. Here only 50% of the interlayered bonds broken in the shear, viz. $(Gd^{3+})_5(Tt_2^{6-})_{1.5}(Tt^{4-})(e^-)_2$ at $x = 2$ [41–43]. We did not find such an intermediate in the $La_5(Ge_{4-x}Si_x)$ system in a less thorough examination. The transformations and related processes among the 5–4 structures carry significant implications with regard to giant magnetocaloric behavior and its applications [44].

Electron distributions and bonding: Applications of simple electron counting schemes and classical models for the anions in the two La_5Ge_3Si structures and to La_5Ge_3Ga result in metallic Zintl phase formulations for all, as follows:

β:Zr_5Si_4-type: $5(La^{3+}) + 2(Tt_2^{6-}) + 3e^- = 0$,
α:Sm_5Ge_4-type: $5(La^{3+}) + 2(Tt^{4-}) + 1(Tt_2^{6-}) + 1e^- = 0$,
Gd_5Si_4-type: $5La^{3+} + Ge_2^{6-} + GeGa^{7-} + 2e^- = 0$.

Two close examples of the first two are La_5Ge_4 and La_5Si_4, respectively (Table 1). The binary tetrelide phases involve an odd number of free electrons in these formulations, whereas the substitution of 25% of the Ge by Ga leads to further dimerization of the La_5Ge_4 parent. Naturally it is to be expected that the compounds La_5Si_3, La_5Si_4, α- and β-La_6Ge_4Si, La_5Ge_3 Ga and others (Table 1) are metallic even according to these oversimplified representations. In fact, numerous lanthanide- or alkaline-earth metal-rich compounds with the tetrels have been observed to deviate stoichiometrically from classical Zintl rules, and many metallic (extra electron) phases with clearly structured Zintl anions now known [45,46] The failure of these overly simple electronic schemes can be attributed to general strong mixing of the lanthanum orbitals with the tetrel states (covalency) that leads to large band widths, even the disappearance of a gap between the tetrel- and the metal-derived bands. A sizeable mixing $5d$ states on lanthanum into the indium valence band in the ideal Zintl phase La_3In_5 (Pu_3Pd_5-type) is evident even according to EHTB calculations as well as in the excess-electron isotypes Sr_3Sn_5 and La_3Sn_5, all of which are metallic [47]. Another possibility is that the multiple tetrelide–tetrelide bonds in formal Tt_2^{6-} ions (isoelectronic with Br_2, etc.) lose their π^* electrons into the conduction band [48].

These earlier suggestions have been put on a firmer footing by the results of recent LMTO–ASA and WIEN2K (DFT) calculations on the Cr_5B_3-type structures of Ae_5Tt_3, Ae = Ca–Ba, Tt = Ge, Sn [49], which in very simple Zintl terms may be represented as closed-shell phases $[(Ae^{2+})_5Tt_2^{6-}Tt^{4-}]$ but which are in fact all metallic. Strong mixing of d orbitals on the 12 cations that surround each Tt_2^{2-} group with its $\rho\pi^*$ states completely eliminate any notion of a closed shell dimer state. It seems clear that these effects will be even greater in the presence of the higher field R^{+3} cations in the present R_5Tt_4 structures, which in fact appear to require excess electrons even by these naive treatments to retain dimer species as observed. This situation may also depend critically on the characteristics of the near-neighbor cation envelope around the dimers and the resulting cation d–dimer $\rho(\pi)$ interactions in other structure types and symmetries. Another example of the Sm_5Ge_4–Gd_5Si_4-type interconversion occurs within the lanthanide elements, namely from the former type for the earlier elements to the latter for Gd_5Si_4, Tb_5Si_4, etc.

The apparent failure of a simple Zintl picture on the La_5Tt_4 compounds and a search for a Zintl-prototype leads us to the rare Eu_5As_4 structure type [6]. Its structure, $Cmca$, can be described as a more symmetric variant of the Sm_5Ge_4 ($Pnma$) structure type with As_2 dimers and pairs of isolated As atoms. (This is not illustrated because its close visual similarity to the

Sm_5Ge_4 analog.) In Eu_5As_4 the M_9Tt_6 units are connected and arranged in the same manner as that found in Sm_5Ge_4 and Gd_5Si_4 except that the arrangement has higher symmetry so that the As atoms form regular octahedra around the central Eu atom. The regular octahedral shape of the $EuAs_6$ fragment now results in (or reflects) the absence of any bonding interactions between the "dangling" As atoms ($d > 4.0$ Å). This is presumably because the structure satisfies the electron count for a Zintl phase with the reasonable expectation that Eu is divalent $[(5Eu^{2+}) + 2As^{3-} + As_2^{4-} = 0]$. However, this electronic situation has evidently not been established experimentally. In practice, judging from our experiences with tetrel dimers, the greater stability of π bonds for As_2^{4-} could lead to a true semiconductor property, as is the case with Sb_2^{4-} in $Na_2Ba_3Sb_4$ [36]. In any case, there has been only one other compound reported as isostructural with Eu_5As_4 on the basis of a single crystal study, β-Ba_5Sb_4, which is presumably a semiconductor too [50]. On the other hand, as Fig. 12 shows, the calculated powder pattern of La_5Ge_4 with the Eu_5As_4 structure is quite similar to the corresponding patterns for the Sm_5Ge_4 and Gd_5Si_4 structure types, particularly the former. The fact that the structures of most reported Sm_5Ge_4-type compounds have been inferred by Debye–Scherrer methods certainly allows for the possibility that some others are actually of the Eu_5As_4 type. β-Ba_5Sb_4 was first misidentified as Gd_5Si_4 type in such a way [50].

The different 5–4 type structures discussed above all have a common structural unit, M_9X_6. In a formal sense, we can also associate this building unit with an analogous anti-type, a stuffed-M_6X_8Z unit found in many metal cluster compounds. The differences between the different 5–4 tetrelide compounds lie on how the M_9X_6 units are interconnected and arranged in space. Dimers are assembled or disassembled according to how the units are interlinked. The structural differentiation between the Zr_5Si_4-type structure and the Sm_5Ge_4-type-related structures might be dominated by size factors
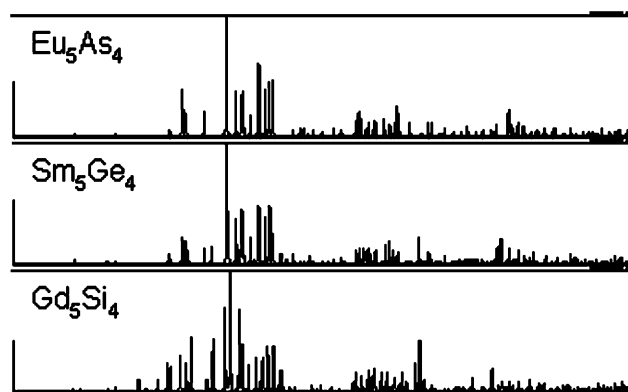

Fig. 12. The calculated powder patterns (4–80°) of La_5Ge_4 for three structure types: (a) Eu_5As_4, (b) Sm_5Ge_4 (actual), (c) Gd_5Si_4.

that affect the packing of the M_9Tt_6 units. Electronic effects in the Zr_5Si_4-types may be of minor significance because a Gd_5Si_4-type arrangement also allows for the dimerization of all the tetrelides. However, the effective tetrahedral packing of the M_9Tt_6 units in Zr_5Si_4 examples leads to smaller coordination spheres around the Tt_2 dimers, which is clearly favored for smaller tetrels.

The Sm_5Ge_4-type arrangement evidently allows more structural variety. Depending on the tendency to form dimers, the Sm_5Ge_4 structure probably accommodates a wider range of electron counts. This occurs particularly in cases in which there are more homoatomic bonds between main-group metalloids than the Zintl counting role would predict. More synthetic, physical, and theoretical studies on ternary and binary rare-earth-metal compounds need to be undertaken to validate the idea. Thus, the structural preference among the various Sm_5Ge_4-type arrangements for tetrels is probably governed by electronic factors that are yet to be completely understood, including strong cation interactions with the hypothetical Tt_2^{6-} dimers, and a clear tendency toward stoichiometrically excess electrons even beyond the overstated values according to classical Zintl phase assignments. The absence of a conduction—valence band gap is perhaps general.

Acknowledgments

References

[1] A.M. Guloy, J.D. Corbett, Inorg. Chem. 32 (1993) 3532.
[2] S. Kauzlarich (Ed.), Chemistry, Structure and Bonding in Zintl Phases and Ions, VCH, New York, 1996.
[3] H.-U. Pfeifer, K. Schubert, Z. Metallkunde 57 (1966) 884.
[4] J.E. Iglesias, H. Steinfink, J. Less-Common Met. 26 (1972) 45.
[5] G.S. Smith, Q. Johnson, A.G. Tharp, Acta Crystallogr. 22 (1967) 269.
[6] Y. Wang, L.D. Calvert, E.J. Gabe, J.B. Taylor, Acta Crystallogr. B 34 (1978) 1962.
[7] V.K. Pecharsky, K.A. Gschneidner Jr., Phys. Rev. Lett. 78 (1997) 4494.
[8] D.H. Ryan, M. Eloueng-Jamroz, J. van Lierop, Z. Altounian, H.B. Wang, Phys. Rev. Lett. 90 (2003) 117202.
[9] C. Magen, Z. Arnold, L. Morellon, Y. Skorokhod, P.A. Algarabel, M.R. Ibarra, M.R.J. Kamarad, Phys. Rev. Lett. 91 (2003) 207202.
[10] K.A. Gschneidner Jr., V.K. Pecharsky, J. Appl. Phys. 85 (1999) 5365.
[11] V.K. Pecharsky, K.A. Gschneidner Jr., J. Appl. Phys. 90 (2001) 4614.
[12] O. Tegus, E. Brück, K.H.J. Buschow, F.R. De Boer, Nature 415 (2002) 150.
[13] A.M. Guloy, J.D. Corbett, Inorg. Chem. 35 (1996) 4669.
[14] A.M. Guloy, J.D. Corbett, Inorg. Chem. 35 (1996) 2616.
[15] D. Hohnke, E. Parthé, Acta Crystallogr. 20 (1966) 572.
[16] A.M. Guloy, Ph.D. Thesis, Iowa State University, 1992.
[17] A.A. Murav'eva, O.S. Zarechnyuk, Inorg. Mater. 6 (1970) 933.
[18] A.M. Guloy, J.D. Corbett, Inorg. Chem. 30 (1991) 4789.
[19] SDP User's Guide, Enraf-Nonius, Delft, Holland, B.A. Frenz and Associates Inc., College Station, TX, 1988.
[20] G.M. Sheldrick, SHELXS-86, Universität Göttingen, Germany, 1986.
[21] N. Walker, D. Stuart, Acta Crystallogr. A 39 (1983) 158.
[22] TEXSAN: Single Crystal Structue Analysis Software, Version 5.0, Molecular Structure Corporation: The Woodlands, TX, 1989.
[23] E. Parthé, L.M. Gelato, Acta Crystallogr. A 40 (1984) 169; L.M. Gelato, E. Parthé, J. Appl. Crystallogr. 20 (1987) 139.
[24] J.D. Corbett, E. Garcia, A.M. Guloy, W.-M. Hurng, Y.-U. Kwon, E.A. Leon-Escamilla, Chem. Mater. 10 (1998) 2824.
[25] W.B. Pearson, The Crystal Chemistry and Physics of Metals and Alloys, Wiley-Interscience, New York, 1972, p. 772.
[26] W.H. Zachariasen, Acta Crystallogr. 2 (1949) 94.
[27] L. Pauling, The Nature of the Chemical Bond, third ed, Cornell University Press, Ithaca, NY, 1960, p. 403.
[28] O.F. Karpinskii, B.A. Evseev, Inorg. Mater. 4 (1968) 1094.
[29] (a) F.C. Frank, J.S. Kasper, Acta Crystallogr. 11 (1958) 184;
(b) B.G. Hyde, S. Andersson, Inorganic Crystal Structures, Wiley, New York, NY, 1989, p. 356.
[30] H.F. Yang, C.H. Reo, G.Y. Liu, Z.W. Ouyang, W.F. Liu, X.M. Feng, W.G. Chu, J.K. Liang, J. Alloys Compd. 361 (2003) 113.
[31] U.Ch. Rodewald, B. Heying, D. Johrendt, R.-D. Hoffman, R. Pöttgen, Z. Naturforsch. 59b (2004) 174.
[32] G.S. Smith, A.G. Tharp, Q. Johnson, Acta Crystallogr. 22 (1967) 940.
[33] K.A. Gschneidner, V.K. Pecharsky, A.O. Pecharsky, V.V. Ivtchenko, E.M. Levin, J. Alloys Compd. 303–304 (2000) 214.
[34] F. Merlo, M.L. Fornasini, Atti Accad. Naz. Lincei, Cl. Sci. Fis. Mat. Nat., Rend. 50 (1971) 186.
[35] F. Merlo, M.L. Fornasini, Atti Accad. Naz. Lincei, Cl. Sci. Fis. Mat. Nat., Rend. 46 (1969) 265.
[36] L. Chi, J.D. Corbett, J. Solid State Chem. 162 (2001) 327.
[37] R. Eisenmann, C. Gieck, U. Rössler, Z. Anorg. Allg. Chem. 625 (1999) 1331.
[38] W. Hönle, J. Lin, M. Hartweg, H.-G. von Schnering, J. Solid State Chem. 97 (1992) 1.
[39] K. Vidyasagar, W. Hönle, H.-G. von Schnering, J. Alloys Compd. 235 (1996) 39.
[40] Y. Mozarivskyj, A.O. Pecharsky, V.K. Pecharsky, K.G. Gschneidner, G J. Miller, unpublished research.
[41] Y. Mozharivskyj, W. Choe, A.O. Pecharsky, G.J. Miller, J. Am. Chem. Soc. 125 (2003) 15183.
[42] W. Choe, V.K. Pecharsky, A.O. Pecharsky, K.G. Gschneidner, V.G. Young, G.J. Miller, Phys. Rev. Lett. 84 (2000) 4617.
[43] W. Choe, A.O. Pecharsky, M. Wörle, G.J. Miller, Inorg. Chem. 42 (2003) 8223.
[44] V.K. Pecharsky, A.P. Holm, K.A. Gschneidner Jr., R. Rink, Phys. Rev. Lett. 91 (2003) 197204.
[45] J.D. Corbett, in: S. Kauzlarich (Ed.), Chemistry, Structure, and Bonding in Zintl Phases and Ions, VCH, New York, 1996 (Chapter 4).
[46] J.D. Corbett, Angew. Chem., Int. Ed. 39 (2000) 670.
[47] M.T. Klem, J.T. Vaughey, J. Harp, J.D. Corbett, Inorg. Chem. 40 (2001) 7020.
[48] E.A. Leon-Escamilla, J.D. Corbett, Inorg. Chem. 40 (2001) 1226.
[49] A.-V. Mudring, J.D. Corbett, J. Am. Chem. Soc. 126 (2004) 5277.
[50] G. Derrien, L. Monconduit, M. Tillard, C. Belin, Acta Crystallogr. C 55 (1999) 1044.